




Nonexponential decay of Feshbach molecules

Francesco V. Pepe ^{1,2} Paolo Facchi ^{1,2} Zeinab Kordi,^{3,2} and Saverio Pascazio ^{1,2,4}

¹*Dipartimento di Fisica and MECENAS, Università di Bari, 70126 Bari, Italy*

²*INFN, Sezione di Bari, 70126 Bari, Italy*

³*Abdus Salam ICTP, 34151 Trieste, Italy*

⁴*Istituto Nazionale di Ottica, CNR, 50125 Firenze, Italy*



(Received 20 September 2019; revised manuscript received 24 December 2019; published 27 January 2020)

We analyze the temporal behavior of the survival probability of an unstable ${}^6\text{Li}$ Feshbach molecule close to the BCS-BEC crossover. We find different instances of nonexponential decay as the magnetic field approaches the resonance value, at which the molecule becomes stable. We observe a transition from an exponential decay towards a regime dominated by a stretched-exponential law.

DOI: [10.1103/PhysRevA.101.013632](https://doi.org/10.1103/PhysRevA.101.013632)

I. INTRODUCTION

The decay of an unstable system is commonly associated with an exponential law. However, the quantum evolution of an unstable state, governed by the Schrödinger equation, features deviations from such a law [1–4]. On one hand, at short times the survival probability is quadratic [5–7]. On the other hand, the exponential regime cannot last indefinitely [8–11], and a slower (typically, power-law) decay takes over at long times (see, however, [12]). In atomic and nuclear physics decays, the aforementioned deviations are usually so small to be practically unobservable, the exponential law having been verified with a high degree of accuracy (see, e.g., [13,14]). The initial quadratic regime of decay, however, has been experimentally confirmed on a number of carefully controlled physical systems [15–22], while the (more elusive) power-law decay at long times has been experimentally confirmed only very recently [23,24].

Strong-coupling effects and/or the presence of a structured spectrum can induce peculiar deviations from the expected exponential law. We will consider here the decay of a weakly bound Feshbach molecule. A Feshbach resonance occurs whenever the energy of the scattering state (two atoms in a given internal configuration, an open channel) is close to the energy of a molecular bound state (a closed channel) [25]. In this situation, the s -wave scattering length diverges, with the molecular state being energetically favored with respect to the unbound atomic state on the side of positive divergence. We will be interested in particular in magnetic resonances, whose control parameter is an external magnetic field. Feshbach resonances give rise to a variety of physical phenomena, including the crossover, at thermal equilibrium, between a BCS state of atomic (fermionic) Cooper pairs and a Bose-Einstein condensation of weakly bound bosonic molecules [26–29], and represents a powerful tool to investigate the atomic structure and interaction potentials [30,31]. The possibility to obtain a stable molecular state by adiabatically varying the magnetic field in the presence of a resonance [32–34], as well as the effects of atom-molecule coherence in the evolution of the system [35,36], has been extensively investigated.

In this article we will consider deviations from exponential decay laws in systems close to Feshbach resonances. For the sake of concreteness, we will focus on the time evolution of an unstable ${}^6\text{Li}$ molecular state [37,38], associated with the resonance at a 543.25 G magnetic field [25,37]. This choice is motivated by the fact that such a resonance is closed-channel dominated, in the sense that, outside the small range of 0.1 G from the resonance, the molecular state has negligible hybridization with the atomic sector. In characterizing the molecule decay, we will unveil the emergence of a stretched-exponential regime [39], which becomes dominant as the resonance is approached.

Dynamics yielding the appearance of stretched exponentials are typical of a number of different phenomena, in both statistical phenomena [39] and glassy dynamics [40], and in the context of one-dimensional Bose gas, when the low-energy physics is well described by a Tomonaga-Luttinger liquid [41]. Interestingly, in the latter case the single-particle correlation function also displays a power-law behavior. Although the coefficients characterizing the stretched exponential can be different, the underlying phenomenon involves the presence of different competing dynamics and lifetimes. We will see that the time evolutions to be discussed in this article have a quantum-mechanical origin and are not amenable to a classical statistical description, being the consequence of the interference of quantum amplitudes.

This article is organized as follows. In Sec. II we introduce the model Hamiltonian and characterize the initial state. In Sec. III we discuss the relation between the Hamiltonian, the molecular state, and the form factors of atom-molecule interactions. In Sec. IV the interatomic potential in the molecular state is approximated by a Morse potential, providing semianalytic results. In Sec. V we introduce the resolvent formalism to characterize the time evolution of the molecule. In Sec. VI we characterize the decay rate of the molecule, in connection with the analytic structure of the propagator of the initial state. In Sec. VII we discuss the different relevant regimes in the time evolution of the molecule. Finally, in Sec. VIII we summarize our results and comment on possible perspectives.

II. HAMILTONIAN AND INITIAL STATE

We will consider the boson-fermion Hamiltonian [42–44]

$$\hat{H} = \hat{H}_0 + \hat{H}_{\text{AM}} + \hat{H}_{\text{F}}, \quad (1)$$

with

$$\hat{H}_0 = \sum_{\mathbf{p}} \sum_{\sigma=\uparrow,\downarrow} \frac{p^2}{2m} \hat{c}_{\mathbf{p},\sigma}^\dagger \hat{c}_{\mathbf{p},\sigma} + \sum_{\mathbf{q}} \left(\frac{q^2}{4m} + E_B \right) \hat{b}_{\mathbf{q}}^\dagger \hat{b}_{\mathbf{q}} \quad (2)$$

describing the dynamics of free fermionic atoms of mass m and bosonic molecules of mass $2m$. Here E_B is the molecular binding energy, which is the difference between the energy of the static resonant molecular state (closed channel) and the continuum threshold for the free-atom pair, which is an approximately linear function of the magnetic field [25]. The field operators $\hat{b}_{\mathbf{q}}$ and $\hat{c}_{\mathbf{p},\sigma}$, which satisfy the canonical (anti)commutation relations

$$[\hat{b}_{\mathbf{q}}, \hat{b}_{\mathbf{q}'}] = 0, \quad [\hat{b}_{\mathbf{q}}, \hat{b}_{\mathbf{q}'}^\dagger] = \delta_{\mathbf{q},\mathbf{q}'}, \quad (3)$$

$$\{\hat{c}_{\mathbf{p},\sigma}, \hat{c}_{\mathbf{p}',\sigma'}\} = 0, \quad \{\hat{c}_{\mathbf{p},\sigma}, \hat{c}_{\mathbf{p}',\sigma'}^\dagger\} = \delta_{\mathbf{p}\mathbf{p}'} \delta_{\sigma\sigma'}, \quad (4)$$

act on the Fock space of the atom-molecule system. The atoms are characterized by two possible internal states (pseudospins), denoted by \uparrow and \downarrow .

The interaction Hamiltonian \hat{H}_{AM} describes the transitions between a pair of atoms with opposite pseudospin and a molecule, preserving the total momentum:

$$\hat{H}_{\text{AM}} = \sum_{\mathbf{K},\mathbf{p}} [G(\mathbf{p}) \hat{b}_{\mathbf{K}}^\dagger \hat{c}_{-\mathbf{p}+\mathbf{K}/2,\downarrow} \hat{c}_{\mathbf{p}+\mathbf{K}/2,\uparrow} + \text{H.c.}] \quad (5)$$

The coupling $G(\mathbf{p})$ between the molecule and the atom pair is assumed to be independent of the total momentum \mathbf{K} by Galilean invariance and reads, according to the second-quantization prescription [45],

$$G(\mathbf{p}) = \langle \psi_{\text{M},0} | H_{\text{int}} | \mathbf{p} \uparrow, -\mathbf{p} \downarrow \rangle, \quad (6)$$

where

$$|\psi_{\text{M},0}\rangle = \hat{b}_0^\dagger |0\rangle, \quad (7)$$

$$|\mathbf{p} \uparrow, -\mathbf{p} \downarrow\rangle = \hat{c}_{\mathbf{p},\uparrow}^\dagger \hat{c}_{-\mathbf{p},\downarrow}^\dagger |0\rangle, \quad (8)$$

with $|0\rangle$ the vacuum of the Fock space and H_{int} the (first-quantization) Hamiltonian that couples the atomic and molecular sectors. We will later characterize the function $G(\mathbf{p})$ for our case study.

The last term in (1) describes the two-body interactions between atoms in different internal states, through an inter-atomic potential that depends only on their relative position:

$$\hat{H}_{\text{F}} = \sum_{\mathbf{p},\mathbf{p}',\mathbf{q}} U(\mathbf{p}-\mathbf{p}') \hat{c}_{\mathbf{p}+\mathbf{q}/2,\uparrow}^\dagger \hat{c}_{-\mathbf{p}+\mathbf{q}/2,\downarrow}^\dagger \hat{c}_{-\mathbf{p}'+\mathbf{q}/2,\downarrow} \hat{c}_{\mathbf{p}'+\mathbf{q}/2,\uparrow}. \quad (9)$$

Since, at low energy, the s -wave contribution dominates the two-body scattering, we will neglect the interactions between atoms in the same internal state, which appear for higher-order partial waves.

Our goal is to characterize the evolution of the initial one-molecule state (7) through its survival probability at

time t ,

$$P(t) = |\langle \psi_{\text{M},0} | e^{-i(t/\hbar)\hat{H}} | \psi_{\text{M},0} \rangle|^2. \quad (10)$$

Note that in experiments with ultracold gases, a molecular condensate can be prepared, represented by a many-body state $|\Psi_0\rangle$ with

$$\langle \Psi_0 | \hat{b}_0^\dagger \hat{b}_0 | \Psi_0 \rangle = N, \quad (11)$$

where typical values of the particle number are $N \simeq 10^4 - 10^7$ [46]. The fraction of molecules out of the condensate is suppressed like $(a_{\text{bg}} n_{\text{mol}})^{1/2}$, where a_{bg} is the background (i.e., far-from-resonance) scattering length and n_{mol} the molecular density. We will assume that, at least in the initial part of the evolution, which is of interest for this article, the effects of intermolecular scattering, mediated by the atom pairs emitted by different molecules, are suppressed. Thus, to a good approximation, the evolved condensate fraction

$$N(t) = \langle \Psi_0 | e^{i(t/\hbar)\hat{H}} \hat{b}_0^\dagger \hat{b}_0 e^{-i(t/\hbar)\hat{H}} | \Psi_0 \rangle \quad (12)$$

will be proportional to the survival probability $P(t)$. In the following, after characterizing the molecular survival probability, we will comment on the range of validity of such an assumption.

III. FORM FACTOR OF THE ATOM-MOLECULE INTERACTION

The atom-molecule form factor is determined by the first-quantization interaction Hamiltonian \hat{H}_{int} and the details of the molecular state $|\psi_{\text{M},0}\rangle$. In order to properly analyze these aspects, we will consider the s -wave Feshbach resonance of ${}^6\text{Li}$ ($m \simeq 10^{-26}$ kg) at $B = B_{\text{res}} = 543.25$ G [25,37]. Since it is an exceptionally narrow (closed-channel-dominated) resonance for a fermionic species, it enables one to create, through an adiabatic sweep of the magnetic field, a system of almost bare molecules, very weakly hybridized with the atomic sectors. The resonance appears in the scattering of atoms in the internal states labeled as the a and b channels, which, in the high-field regime [25], safely applicable at B_{res} , coincide with

$$|\uparrow\rangle \equiv |i_z = 1, s_z = -1/2\rangle, \quad (13)$$

$$|\downarrow\rangle \equiv |i_z = 0, s_z = -1/2\rangle, \quad (14)$$

where i_z and s_z are the components along the magnetic field of the atomic nuclear and electronic spin, respectively, in units of \hbar . Henceforth, we will adopt the notation

$$\mathbf{S} = \mathbf{s}_1 + \mathbf{s}_2, \quad \mathbf{I} = \mathbf{i}_1 + \mathbf{i}_2 \quad (15)$$

for the total spins.

The atom-pair state $|\mathbf{p} + \mathbf{K}/2 \uparrow, -\mathbf{p} + \mathbf{K}/2 \downarrow\rangle$ can be decomposed into the product of the center-of-mass state $|\mathbf{K}_{\text{c.m.}}\rangle$ and an antisymmetric relative-motion state $|\mathbf{p} \uparrow, -\mathbf{p} \downarrow\rangle$, defined in (8), which reads, in terms of the orbital and internal states,

$$|\mathbf{p} \uparrow, -\mathbf{p} \downarrow\rangle = \frac{1}{\sqrt{2}} (|\mathbf{p}, -\mathbf{p}\rangle_- \otimes |\psi_{ab}^+\rangle + |\mathbf{p}, -\mathbf{p}\rangle_+ \otimes |\psi_{ab}^-\rangle), \quad (16)$$

where

$$\begin{aligned} |\psi_{ab}^{\pm}\rangle &= \frac{1}{\sqrt{2}}(|\uparrow\rangle \otimes |\downarrow\rangle \pm |\downarrow\rangle \otimes |\uparrow\rangle), \\ |\mathbf{p}, -\mathbf{p}\rangle_{\pm} &= \frac{1}{\sqrt{2}}(|\mathbf{p}\rangle \otimes |-\mathbf{p}\rangle \pm |-\mathbf{p}\rangle \otimes |\mathbf{p}\rangle). \end{aligned} \quad (17)$$

Notice that, while the pseudospin state can be either symmetric or antisymmetric, the atom pair is always an *electronic spin* triplet state, corresponding to $S_z = -1$. The resonant bound state is an *s*-wave electronic spin singlet state, whose nuclear spin is a quasidegenerate mixture of $I = 0$ and $I = 2$ [25]. The state $|\psi_{M,K}\rangle$ of the molecule can thus be factorized into

$$|\psi_{M,K}\rangle = |\mathbf{K}_{c.m.}\rangle \otimes |\phi_M\rangle \otimes |\Phi_I\rangle \otimes |S = 0, S_z = 0\rangle, \quad (18)$$

where $|\phi_M\rangle$ is the spherically symmetric orbital wave function and $|\Phi_I\rangle$ the superposition of the $I = 0, 2$ states coupled to the atom-pair state by H_{int} . The open and closed channels are connected by the hyperfine coupling [35] between the nuclear and electronic spins of each atom

$$H_{\text{int}} \equiv H_{\text{hf}} = A_{\text{hf}}(\mathbf{i}_1 \cdot \mathbf{s}_1 + \mathbf{i}_2 \cdot \mathbf{s}_2), \quad (19)$$

where the constant A_{hf} can be deduced from the hyperfine splitting between the states with total spin $f = 3/2$ and $f = 1/2$ at zero magnetic field. In the case of ${}^6\text{Li}$, the hyperfine splitting reads $\delta E_{\text{hf}}/\hbar = 228$ MHz and its relation to the coupling constant is $A_{\text{hf}} = (2/3)\delta E_{\text{hf}}$.

Since the hyperfine Hamiltonian does not act on the relative motion degrees of freedom, only the term involving $|\mathbf{p}, -\mathbf{p}\rangle_+$ in the pair wave function is coupled to the *s*-wave bound state and contributes to $G(\mathbf{p})$ in (6). The action of the hyperfine Hamiltonian on the related pseudospin state $|\psi_{ab}^-\rangle$ reads

$$\begin{aligned} \frac{1}{A_{\text{hf}}} H_{\text{hf}} |\psi_{ab}^-\rangle &= -\frac{1}{2} |\psi_{ab}^-\rangle + \frac{1}{2} |I = 1, I_z = 0\rangle \otimes |\tau\rangle \\ &+ \frac{\sqrt{3}}{6} (|I = 2, I_z = 0\rangle - 2\sqrt{2}|I = 0, I_z = 0\rangle) \\ &\otimes |\sigma\rangle, \end{aligned} \quad (20)$$

with $|\tau\rangle \equiv |S = 1, S_z = 0\rangle$ and $|\sigma\rangle \equiv |S = 0, S_z = 0\rangle$. Assuming that the initial molecule condensate is obtained from free atoms by adiabatically sweeping the magnetic field across the resonance, the bound nuclear state in (18) can be identified by the normalized state

$$|\Phi_I\rangle = \frac{1}{3} |I = 2, I_z = 0\rangle - \frac{2\sqrt{2}}{3} |I = 0, I_z = 0\rangle \quad (21)$$

associated with the electronic spin singlet $|\sigma\rangle$ in (20). Based on these considerations, the form factor of the atom-molecule interaction in (5) reads

$$\begin{aligned} G(\mathbf{p}) &= \frac{1}{\sqrt{2}} \langle \phi_M | \mathbf{p}, -\mathbf{p} \rangle_+ (\langle \sigma | \otimes \langle \Phi_I |) H_{\text{hf}} | \psi_{ab}^- \rangle \\ &= \frac{\sqrt{3}}{2} A_{\text{hf}} \frac{\tilde{\phi}_M(\mathbf{p})}{\sqrt{V}}, \end{aligned} \quad (22)$$

with V the quantization volume, $\phi_M(\mathbf{r}) = \langle \mathbf{r} | \phi_M \rangle$, and

$$\tilde{\phi}_M(\mathbf{p}) = \int d\mathbf{r} \phi_M(\mathbf{r}) e^{i\mathbf{p}\cdot\mathbf{r}/\hbar}. \quad (23)$$

To determine an explicit expression for the Fourier-transformed molecular orbital wave function $\tilde{\phi}_M$, we will consider in the following section an approximated interatomic potential.

IV. MORSE POTENTIAL APPROXIMATION

The resonant molecular state is the last excited vibrational state, with vibrational quantum number $v = 38$, of the interatomic potential in the electronic spin singlet state. Since its wave function is spherically symmetric, a radial wave function $\chi(r)$, with $r = |\mathbf{r}|$, can be used,

$$\phi_M(\mathbf{r}) = \frac{\chi(r)}{r}. \quad (24)$$

The radial equation can be solved if the interatomic potential, characterized by a repulsive core and an attractive tail, is approximated by a Morse potential

$$V(r) = D(e^{-2\alpha(r-r_0)} - 2e^{-\alpha(r-r_0)}), \quad (25)$$

which depends on three parameters: the absolute value of the minimum D , the radial distance r_0 of the minimum, and the inverse length constant α . The discrete negative energy levels are characterized by an integer vibrational quantum number v , ranging from zero to $[\lambda]$, with

$$\lambda = \frac{\sqrt{2\mu D}}{\hbar\alpha}, \quad (26)$$

where μ is the reduced mass, and read

$$\epsilon(v) = -\frac{(\hbar\alpha)^2}{2\mu} \left(\lambda - v - \frac{1}{2} \right)^2. \quad (27)$$

The independent parameters λ , α , and r_0 can be fixed by fitting the relevant features of the physical state, namely, the potential depth $V_{\text{min}}/\hbar = 250$ THz, the dissociation energy $E_{38}/\hbar \simeq 1.6$ GHz, the potential minimum position $r_0 \simeq 5a_0$, with $a_0 = 5.29 \times 10^{-11}$ m the Bohr radius, and the classical turning points $a_{\text{min}} \simeq 3a_0$ and $a_{\text{max}} \simeq 43a_0$. We choose the three parameters of the Morse potential by preserving the following features of the measured potential: the ratio of the binding energy to the potential depth, the extension of the classical motion for $v = 38$, and the position of the inner turning point. This ensures an accurate reproduction of the spatial distribution of the state. The ratio E_{38}/V_{min} fixes the parameter λ by imposing

$$\frac{|\epsilon(38)|}{D} = \frac{1}{\lambda^2} \left(\lambda - 38 - \frac{1}{2} \right)^2 = \frac{E_{38}}{V_{\text{min}}} \Rightarrow \lambda \simeq 38.6, \quad (28)$$

while α is determined in terms of E_{38} and $\delta r = a_{\text{max}} - a_{\text{min}}$ through

$$\alpha = \frac{1}{\delta r} \ln \left(\frac{1 + \sqrt{1 - E_{38}/V_{\text{min}}}}{1 - \sqrt{1 - E_{38}/V_{\text{min}}}} \right) \simeq \frac{1}{3a_0}. \quad (29)$$

The minimum of the approximate potential is placed at

$$r_0 = r_{\text{min}} + \frac{1}{\alpha} \ln \left(1 + \sqrt{1 - \frac{E_{38}}{V_{\text{min}}}} \right) \simeq 5.08a_0, \quad (30)$$

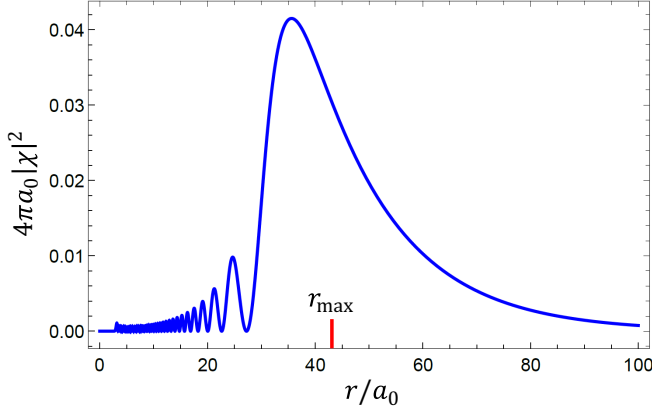


FIG. 1. Morse approximation of the radial probability density $4\pi|\chi(r)|^2$. The red tick represents the outer turning point of the classical motion at energy E_{38} .

remarkably close to the measured value. Since $[\lambda] = 38$, the resonant state considered here is the most excited discrete level in the Morse potential, as in the real case.

We can determine the wave function ψ_{38} , depending on the dimensionless variable $x = \alpha r$, as

$$\begin{aligned} \psi_{38}(x) &= N_{\lambda,38}(y(x))^{\lambda-77/2} e^{-y(x)/2} L_{38}^{2\lambda-77}(y(x)), \\ N_{\lambda,38} &= \sqrt{\frac{38!(2\lambda-77)}{\Gamma(2\lambda-38)}}, \\ y(x) &= 2\lambda e^{-(x-\alpha r_0)}, \end{aligned} \quad (31)$$

where $\Gamma(\beta)$ is the Euler Gamma function and $L_{\gamma}^{\delta}(z)$ is a generalized Laguerre polynomial, satisfying

$$\int_0^{\infty} dx |\psi_{38}(x)|^2 = 1. \quad (32)$$

To obtain the correct normalization of the molecular wave function $\phi_M(\mathbf{r})$, the radial function $\chi(r)$ must be related to (31) by

$$\chi(r) = \sqrt{\frac{\alpha}{4\pi}} \psi_{38}(y(\alpha r)). \quad (33)$$

The radial wave function, plotted in Fig. 1, is evidently concentrated around the outer classical turning point and is significantly extended beyond it. The Fourier transform (23) of the molecular wave function, once the spherical symmetry of $\phi_M(\mathbf{r})$ is exploited and the $V \rightarrow \infty$ limit is taken, can be conveniently expressed in terms of an integral involving the adimensional wave function (31),

$$\tilde{\phi}_M(\mathbf{p}) = \frac{4\pi\hbar}{p} \int_0^{\infty} dr \chi(r) \sin\left(\frac{pr}{\hbar}\right) = \sqrt{\frac{4\pi}{\alpha}} \frac{\hbar}{p} F\left(\frac{p}{\hbar\alpha}\right), \quad (34)$$

with

$$F(P) \equiv \int_0^{\infty} dx \psi_{38}(z(x)) \sin(Px). \quad (35)$$

The behavior of the form factor $G(\mathbf{p})$, which is proportional to $\tilde{\phi}_M(\mathbf{p})$, is determined by the adimensional function $F(P)/P$.

At low momenta, the form factor approaches a constant, since

$$\frac{F(P)}{P} \rightarrow I_1 \equiv \int_0^{\infty} dx \psi_{38}(z(x)) x \simeq 94. \quad (36)$$

The square of $F(P)/P$ falls off rapidly with P and is fitted to a very good approximation by a Gaussian function $I_1 \exp[-(\alpha b P)^2]$, where $b \simeq 46.7a_0$ can be interpreted as a cutoff length.

V. SELF-ENERGY AND DYNAMICS

The survival probability amplitude of the initial one-molecule state (7), $|\psi_{M,0}\rangle = \hat{L}_0^{\dagger}|0\rangle$, reads, for $t > 0$,

$$\mathcal{A}(t) = \langle \psi_{M,0} | e^{-iHt/\hbar} | \psi_{M,0} \rangle = \frac{i}{2\pi} \int_{\mathcal{B}} dE \mathcal{G}(E) e^{-iEt/\hbar}, \quad (37)$$

where the propagator

$$\mathcal{G}(E) = \langle \psi_{M,0} | \frac{1}{E - H} | \psi_{M,0} \rangle \quad (38)$$

is the expectation value of the resolvent $(E - H)^{-1}$ in the initial state $|\psi_{M,0}\rangle$, and the integration (Bromwich) path \mathcal{B} is a horizontal line in the complex energy upper half plane, $\text{Im } E > 0$, with a constant imaginary part, in accord with the convergence of the Fourier transform (37). The propagator can be expressed as

$$\mathcal{G}(E) = \frac{1}{E - E_B - \Sigma(E)}, \quad (39)$$

with E_B the binding energy of the bare molecule and $\Sigma(E)$ the self-energy, representing all possible transitions generated by the interaction Hamiltonian H_{hf} and connecting $|\psi_{M,0}\rangle$ with itself, without involving $|\psi_{M,0}\rangle$ as an intermediate state.

The self-energy can always be expressed as an integral involving a spectral function $\kappa(E)$ as

$$\Sigma(E) = \int_{E_0}^{\infty} dE' \frac{\kappa(E')}{E - E'} \quad (40)$$

for $E \in \mathbb{C} \setminus [E_0, +\infty)$, with E_0 the ground energy of H . If one neglects, as a first approximation, the scattering between free atoms [namely, $U(\mathbf{p}) = 0$ in Eq. (9)], the spectral function [47] can be computed exactly and reads

$$\kappa^0(E) = \sum_{\mathbf{p}} |\langle \mathbf{p} \uparrow, -\mathbf{p} \downarrow | \hat{H}_{\text{AM}} | \psi_{M,0} \rangle|^2 \delta(E - E_{\mathbf{p}}), \quad (41)$$

with $E_{\mathbf{p}} = p^2/m$ the energy of a pair of atoms with mass m and opposite momenta \mathbf{p} and $-\mathbf{p}$ and where the superscript 0 will henceforth label the zeroth-order approximation (in U). After a straightforward manipulation, one obtains

$$\begin{aligned} \kappa^0(E) &= \sum_{\mathbf{p}} |G(\mathbf{p})|^2 \delta(E - E_{\mathbf{p}}) \\ &= \frac{3A_{\text{hf}}^2}{4\pi\hbar\alpha} \sqrt{\frac{m}{E}} F^2\left(\frac{\sqrt{mE}}{\hbar\alpha}\right) \theta(E), \end{aligned} \quad (42)$$

with F defined in Eq. (35). It is evident that $\kappa^0(E) = 0$ if E does not belong to the continuous spectrum of the

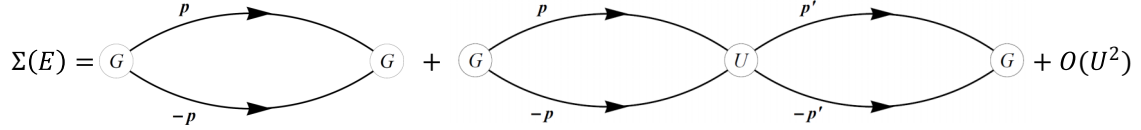


FIG. 2. Feynman diagrams of the contributions to the self-energy $\Sigma(E)$ of the molecular state up to second order in U . Each pair of lines represents a free-atom-pair propagator $E - p^2/m$, while the functions G and U must be computed taking into account the momenta of the propagators connected to the specific vertex.

free-fermion Hamiltonian. Based on the expression (35), the spectral function also reads

$$\kappa^0(E) = \sqrt{E} f(E) \theta(E), \quad (43)$$

where $f(E)$ is a single-valued function, analytic on the whole complex plane. Thus, at low energy, the functional form of the spectral function is determined only by the density of states. Let us recall that the spectral function is related to the (approximate) inverse lifetime of the molecular state with binding energy E_B by the Fermi golden rule

$$\gamma_{\text{GR}}(E_B) = \frac{2\pi}{\hbar} \kappa^0(E_B), \quad (44)$$

which is nonzero only when E_B is positive. The integral (40), providing the self-energy Σ^0 , is well defined on the whole complex plane except for the positive real axis, on which a branch cut is present [47].

Interatomic scattering renormalizes the two-atom propagator appearing in the self-energy of the molecule [42], introducing new processes that change the momenta of the emitted atom pair before recombination. Let us analyze how these processes, diagrammatically represented in Fig. 2, affect the self-energy. Consider, for simplicity, the case in which the coupling between the atom pair and the molecule is constant

$$G \equiv G(0) = \frac{\sqrt{3}}{2\sqrt{V}} A_{\text{hf}} \tilde{\phi}_{\text{M}}(0) = \sqrt{\frac{3\pi}{V}} I_1 \frac{A_{\text{hf}}}{\alpha^{3/2}}, \quad (45)$$

as well as the interatomic coupling $U \equiv U(0)$, physically related to the background scattering length $a_{\text{bg}} \simeq 60a_0$ (namely, the scattering length far from the Feshbach resonance) by [48]

$$U = \frac{U_c}{V} \left(1 - \frac{\sqrt{\pi}b}{a_{\text{bg}}}\right)^{-1} \quad \text{with} \quad U_c \equiv -\frac{4\pi^{3/2}\hbar^2 b}{m}. \quad (46)$$

In the last equality, V is the normalization volume and b the characteristic length of a Gaussian cutoff function, which has been used to regularize $O(a_{\text{bg}}^2)$ terms, the first-order term being the usual result $4\pi\hbar^2 a_{\text{bg}}/m$. We will effectively assume that the form factor of interatomic scattering has the same cutoff length as the atom-molecule transition (see, e.g., Ref. [48]). Incidentally, we observe that, since $U > 0$, no BCS transition is expected at low temperature.

The self-energy in the absence of scattering reads

$$\Sigma^{(0)}(E) = \Sigma^0(E) = \sum_p \frac{G^2}{E - E_p}, \quad (47)$$

while the first-order term in U is

$$\Sigma^{(1)}(E) = \sum_p \frac{G}{E - E_p} U \sum_{p'} \frac{G}{E - E_{p'}} = \frac{U}{G^2} [\Sigma^0(E)]^2. \quad (48)$$

Notice that, since $G \propto V^{-1/2}$ and $U \propto V^{-1}$, the ratio U/G^2 is independent of the normalization volume V . Since the n th-order term in U reads

$$\Sigma^{(n)}(E) = \Sigma^0(E) \left(\frac{U}{G^2} \Sigma^0(E) \right)^n, \quad (49)$$

it is possible to sum all the contributions to the self-energy and get

$$\Sigma(E) = \sum_{n=0}^{\infty} \Sigma^{(n)}(E) = \frac{\Sigma^0(E)}{1 - \frac{U}{G^2} \Sigma^0(E)}. \quad (50)$$

This result represents a special case, in vacuum and for a short-range potential, of the scattering t -matrix computation [45,49]. The divergent $\Sigma^0(E)$ is regularized by the replacement $G \rightarrow G(\mathbf{p})$. The complete spectral function can be obtained by making use of the identity $\text{Im} \Sigma(E + i0^+) = -\pi \kappa(E)$, which yields

$$\kappa(E) = \frac{\kappa^0(E)}{\left[1 - \frac{U}{G^2} \text{P} \int_0^{\infty} dE' \frac{\kappa^0(E')}{E - E'}\right]^2 + \left[\frac{U}{G^2} \pi \kappa^0(E)\right]^2}, \quad (51)$$

with $\text{P} \int$ denoting principal value integration. The new function $\kappa(E)$ inherits the square-root singularity of $\kappa^0(E)$.

To determine the decay rate, one performs the analytic continuation of the self-energy from the upper to the lower complex half plane, through the branch cut. The continuation results in the expression for the self-energy on the second Riemann sheet

$$\Sigma_{\text{II}}(E) = \Sigma(E) - 2\pi i \kappa(E), \quad \text{Im} E < 0, \quad (52)$$

with $\kappa(E)$ the analytic continuation of the spectral function from the positive real axis. The decay rate and wave-function renormalization are determined by the pole of the propagator (38) in the lower half plane of the second Riemann sheet, which satisfies

$$E_{\text{pole}} = E_B + \Sigma_{\text{II}}(E_{\text{pole}}), \quad (53)$$

and can be considered as a function of the binding energy that, close to the resonance, is approximately linear in the magnetic field

$$E_B(B) = 2\mu_{\text{Bohr}}(B - B_0), \quad (54)$$

with $\mu_{\text{Bohr}} = 9.27 \times 10^{-24}$ J/T the Bohr magneton and B_0 the value at which the bare binding energy is equal to the

continuum threshold of the atom pair. The linear dependence is due to the Zeeman splitting between the bound state, which is an electronic singlet, and the free state, characterized by $S_z = -1$ [see Eqs. (13) and (14)]. Once the pole has been determined, the survival amplitude in the initial state can be split as

$$\mathcal{A}(t) = Z e^{-i(E_B + \Delta E)t/\hbar} e^{-\gamma t/2} + \tilde{\mathcal{A}}(t), \quad (55)$$

where the first term, giving an exponential decay, is related to the integration around the pole, while the second term $\tilde{\mathcal{A}}$ contains residual contributions from branch cut integrations and is responsible for all deviations from the exponential law [4,47]. The energy shift ΔE and the decay rate γ of the bound state are related to the real and imaginary parts of the pole by

$$\Delta E = \text{Re } E_{\text{pole}}, \quad \gamma = -\frac{2}{\hbar} \text{Im } E_{\text{pole}}. \quad (56)$$

The amplitude factor Z , also known as the wave-function renormalization, is the residue at the pole, related to the first derivative of the self-energy by

$$Z = \left[\frac{dG^{-1}}{dE}(E_{\text{pole}}) \right]^{-1} = \frac{1}{1 - \Sigma'_{\text{II}}(E_{\text{pole}})} = \frac{dE_{\text{pole}}(E_B)}{dE_B}, \quad (57)$$

where the last equality follows from the pole definition (53) and the prime denotes derivative.

VI. POLES OF THE PROPAGATOR

The analytic properties of the propagator (38), discussed in the preceding section, provide the basis to characterize the stability properties of the molecular state with varying binding energy E_B . If the binding energy is significantly smaller than zero, we expect the molecular state to be stable and very well approximated by $|\psi_{M,0}\rangle$, while hybridization with the atomic sector will increase as the magnetic field approaches the resonance. When the molecule is stable, a real pole, representing the energy of the dressed molecular state, can be found on the first Riemann sheet, at an energy smaller than the branching point at $E = 0$. Actually, real negative solutions of the equation

$$E_{\text{pole}} = E_B(B) + \Sigma(E_{\text{pole}}) \quad (58)$$

are found up to the value B_{res} of magnetic field such that

$$E_B(B_{\text{res}}) + \Sigma(0) = 0 \Rightarrow B_{\text{res}} - B_0 = 0.208 \text{ G}. \quad (59)$$

As B approaches B_{res} from below, the derivative $\Sigma'(E_{\text{pole}})$ diverges due to the singularity of the spectral function in E_0 . Thus the quantity $Z(E_B)$, defined as in (57) on the second Riemann sheet, vanishes. Therefore, approaching the resonance from below, E_{pole} admits the quadratic approximation

$$E_{\text{pole}}(E_B) \sim 2\mu_B^2 \eta (B - B_{\text{res}})^2, \quad (60)$$

as $B \uparrow B_{\text{res}}$, with (the prime and double primes denote derivatives)

$$\eta \equiv \left. \frac{dZ(E_B)}{dE_B} \right|_{B \uparrow B_{\text{res}}} = \lim_{\epsilon \uparrow 0} \frac{\Sigma''(\epsilon)}{[1 - \Sigma'(\epsilon)]^3}, \quad (61)$$

while it is linear far from the resonance. The very small width found for the pure quadratic region ($\lesssim 10^{-6}$ G) is expected from the extreme narrowness of the resonance. The value B_{res} represents the actual position of the resonance, which is an experimental parameter and not a prediction of the model. Close to the resonance, the energy of the bound state is related to the positively diverging scattering length $a(B)$ by [25]

$$|E_{\text{pole}}| \simeq \frac{\hbar^2}{ma^2(B)} \Rightarrow a^2(B) \simeq \frac{\hbar^2}{2\mu_B^2 |\eta| m (B - B_{\text{res}})^2}. \quad (62)$$

Comparing this relation with the general expression [25,38]

$$a(B) = a_{\text{bg}} \left(1 - \frac{\Delta}{B - B_{\text{res}}} \right) \quad (63)$$

of the resonant scattering length, one obtains the result $\Delta \simeq 0.08$ G, which is very close to the measured value [37].

The zeros of

$$\mathcal{G}_{\text{II}}(E)^{-1} = E - E_B - \Sigma_{\text{II}}(E), \quad (64)$$

with $\text{Im } E < 0$, are the poles of the propagator on the second Riemann sheet, which are relevant for the decay dynamics. The time-reversed process is instead related to the zeros of $\mathcal{G}_{\text{II}}(E)^{-1}$ in the upper half plane, $\text{Im } E > 0$, where one gets

$$\Sigma_{\text{II}}(E) = \Sigma(E) + 2\pi i \kappa(E), \quad (65)$$

which coincides with the analytical continuation of $\Sigma(E)$ from below the branch cut on the first Riemann sheet. Indeed, due to the square-root singularity of the spectral function, the two expressions (52) and (65) of Σ_{II} coincide on the negative real axis, since $\sqrt{x + i0^+} = -\sqrt{x - i0^+}$ for $x < 0$.

On the negative axis of the second Riemann sheet a real pole with $Z > 0$, solution of

$$E_{\text{pole}} = E_B(B) + \Sigma(E_{\text{pole}}) + 2\pi i \kappa(E_{\text{pole}} + i0^+), \quad (66)$$

exists for all $B < B_{\text{res}}$ and moves towards the origin as B increases. As we have seen before, also the pole on the negative real axis of the first Riemann sheet (58) moves towards the origin as B increases. At $B = B_{\text{res}}$ it hits the branch point at the origin and bounces back on the second Riemann sheet moving backward on the negative real axis as B increases. The two real poles on the second Riemann sheet collide at $B = B_1$, with

$$B_1 \simeq B_{\text{res}} + 2.64 \times 10^{-5} \text{ G}, \quad (67)$$

bouncing off each other and generating two complex conjugate poles, in the lower and upper half planes. The locus of the poles in the second Riemann sheet is shown in Fig. 3, with the arrows pointing toward increasing magnetic field. The real part of the complex poles increases linearly with $B - B_1$ for all $B > B_1$, while their imaginary parts scale approximately like $\sqrt{B - B_1}$.

The imaginary part of the complex pole in the lower half plane yields the decay rate γ of the unstable molecule through (56), which is plotted in Fig. 4. The lifetime is considerably shifted with respect to the Fermi golden rule result (44), obtained from the spectral density at $U = 0$, since, close to the crossing ($B \sim B_0$), the atom-molecule coupling can no longer be treated as a perturbation.

The squared modulus of the wave-function renormalization Z in Eq. (55) represents the extrapolation of the exponential

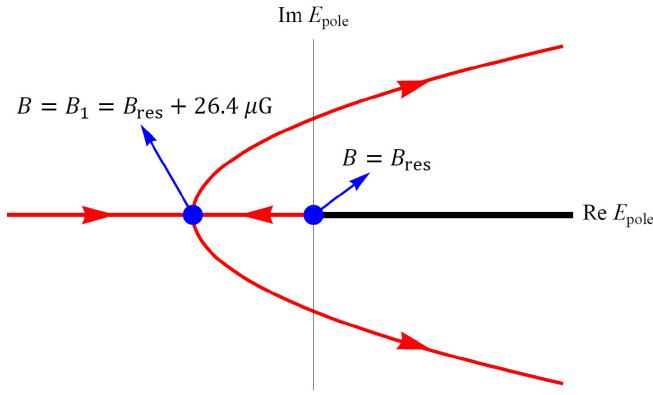


FIG. 3. Locus of the poles of the propagator of the initial state $|\psi_{M,0}\rangle$ in the second Riemann sheet. The poles in the lower half plane ($\text{Im } E < 0$) are solution of the equation $E_{\text{pole}} = E_B + \Sigma(E_{\text{pole}}) + 2\pi i\kappa(E_{\text{pole}})$, while the poles in the upper half plane ($\text{Im } E > 0$) satisfy $E_{\text{pole}} = E_B + \Sigma(E_{\text{pole}}) - 2\pi i\kappa(E_{\text{pole}})$. The two equations coincide for real negative poles. The second pole on the negative real axis originates from a negative pole on the first Riemann sheet which passes through the origin for $B = B_{\text{res}}$. The two real poles collide and bounce off into two complex conjugate poles for $B = B_1 = B_{\text{res}} + 26.4 \mu\text{G}$. The arrows on the red lines show the motion of poles as the magnetic field increases.

part of the survival probability back to the time origin $t = 0$,

$$P(t) = |\mathcal{A}(t)|^2 \simeq |Z|^2 \exp(-\gamma t). \quad (68)$$

The plot in Fig. 5 shows that for $B - B_{\text{res}} \lesssim 10^{-2}$ G, the value of $|Z|^2$ is significantly larger than one (which is only possible for unstable states [50]) and diverges as B approaches B_1 from above like $(B - B_1)^{-1/2}$. Incidentally, we notice that wave-function renormalization effects have been experimentally observed in [23,24,51].

VII. TIME EVOLUTION

The increasing value of $|Z|^2$ as the system approaches the resonance is a marker of the strong deviation of the molecular

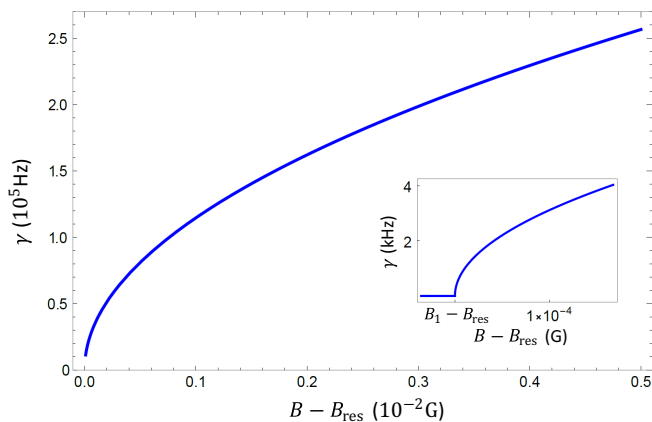


FIG. 4. Inverse lifetime γ of the unstable molecule for $B > B_{\text{res}}$. The inset shows a close-up of the region close to $B = B_{\text{res}}$, where, even though the decay rate vanishes for $B_{\text{res}} < B < B_1$, the molecule is still unstable.

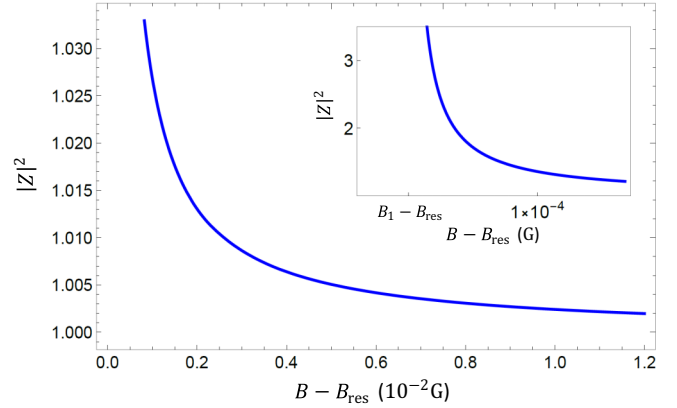


FIG. 5. Square modulus $|Z|^2$ of the wave-function renormalization Z in (55). Here $|Z|^2$ coincides with the extrapolated value at $t = 0$ of the exponential part of the molecule survival probability and diverges like $(B - B_1)^{-1/2}$ at $B = B_1 > B_{\text{res}}$.

survival probability $P(t)$ from an exponential law. Generally, in the absence of bound states, the survival probability can be written as

$$P(t) = |\mathcal{A}(t)|^2 = \left| \int_0^\infty dE \omega(E) e^{-iEt/\hbar} \right|^2, \quad (69)$$

with

$$\omega(E) = \frac{\kappa(E)}{(E - E_B - P \int_0^\infty dE' \frac{\kappa(E')}{E - E'})^2 + \pi^2 \kappa(E)^2} \geq 0, \quad (70)$$

where the energy density $\omega(E) = -\text{Im } \mathcal{G}(E + i0^+)/\pi$ is obtained from (37), (39), and (40) (we set $E_0 = 0$) by deforming the Bromwich path \mathcal{B} around the branch cut on the positive real axis. The positive denominator of $\omega(E)$ is smaller when the energy E gets closer to a pole in the second Riemann sheet.

In the perturbative regime, deviations from the exponential law are usually expected for very short times (Zeno region), where the behavior of the survival probability must be quadratic, and for very long times, where a power-law tail supersedes the vanishing exponential part. In our system, a peculiar structure of the decay law emerges close to the resonance, which is mainly due to the form of the spectral function, scaling like \sqrt{E} for practically the whole relevant energy range.

In order to analyze the effects we discussed close to resonance and quantify the nonexponentiality of decay, let us compare the plots in Fig. 6. In Fig. 6(a), corresponding to the case $B - B_{\text{res}} = 12$ mG, the computed survival probability is characterized by $|Z|^2 \simeq 1.002$ and $\gamma \simeq 4 \times 10^4 \text{ s}^{-1}$ and approaches the asymptotic curve $|Z|^2 e^{-\gamma t}$ after a time $\simeq 1/3\gamma$. Figure 6(b) represents the case $B - B_{\text{res}} = 0.92$ mG, a situation in which the complex pole is very close to the real axis, with $|Z|^2 \simeq 1.03$ and $\gamma \simeq 1 \times 10^4 \text{ s}^{-1}$. In the latter case, the survival probability intersects the asymptotic exponential at a time very close to $1/\gamma$, where the survival probability is already reduced by more than $1/2$. As the magnetic field approaches B_1 from above, the first intersection between $P(t)$ and $|Z|^2 e^{-\gamma t}$ tends to infinity. Thus, in the limit $B \downarrow B_1$, the

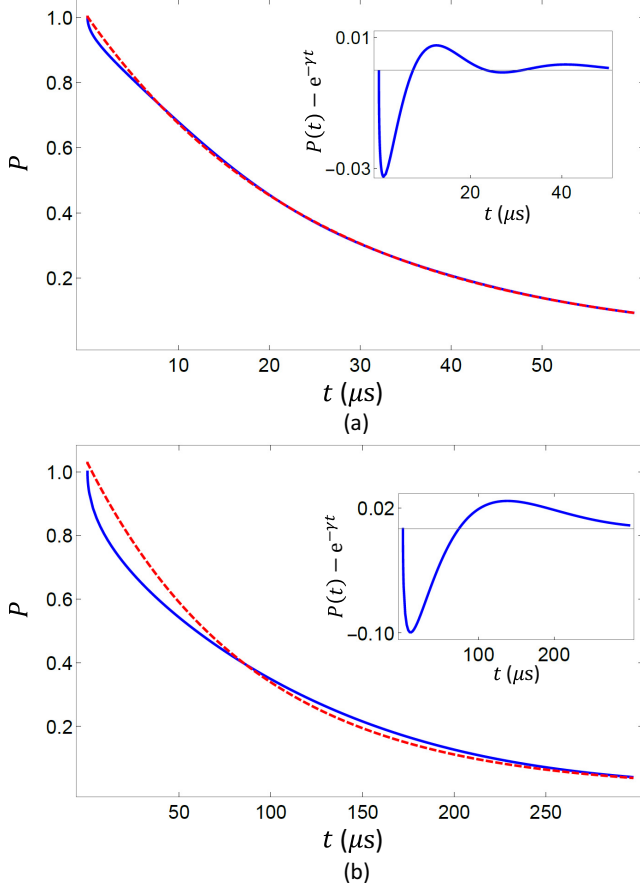


FIG. 6. Nonexponential decay at short times for $B > B_1$ in the cases (a) $B - B_{\text{res}} = 12$ mG and (b) $B - B_{\text{res}} = 0.92$ mG. In case (a), $\gamma = 3.96 \times 10^4 \text{ s}^{-1}$ and $|Z|^2 - 1 = 2 \times 10^{-3}$; in case (b), $\gamma = 1.11 \times 10^4 \text{ s}^{-1}$ and $|Z|^2 - 1 = 2.8 \times 10^{-2}$. The blue solid lines represent the exact survival probability $P(t)$ of the molecule, approaching the asymptotic red dashed curves $|Z|^2 \exp(-\gamma t)$ after a transient. If the magnetic field is very close to resonance, nonexponentiality is enhanced and the intersection point between the survival probability and the asymptotic exponential moves towards $t \rightarrow \infty$. In the insets, the difference between the survival probability and a pure exponential curve with lifetime $1/\gamma$ is plotted.

exponential regime is never reached and a new decay law emerges. Note that this law does not correspond to the initial quadratic regime, which is practically unresolved in the plots, since the curvature of $P(t)$ at the origin is given by the Zeno time $\tau_Z = \hbar / \langle \psi_{M,0} | H_{AM}^2 | \psi_{M,0} \rangle^{1/2} \simeq 10$ ns, while the validity of the quadratic approximation holds for $t \lesssim 2mb^2/\hbar \simeq 1$ ns.

An analysis of the time evolution of molecules in the intermediate range $B_{\text{res}} < B < B_1$ enables one to characterize the emergent decay law. Indeed, the square-logarithmic plot in Fig. 7 shows that, in this intermediate magnetic field range, decay is characterized by an approximate stretched-exponential law

$$P(t) \simeq e^{-at^\beta}, \quad (71)$$

with β very close to $1/2$. The physical origin of such behavior can be ascribed to the fact that, for $B_{\text{res}} < B < B_1$ and times much larger than the inverse frequency cutoff $2mb^2/\hbar$, the

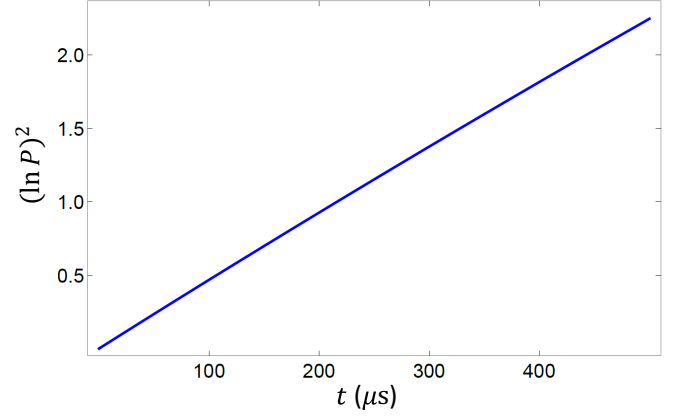


FIG. 7. Squared logarithm of the molecular survival probability for $B - B_{\text{res}} = 18 \mu\text{G}$. In the intermediate region $B_{\text{res}} < B < B_1$, in which the molecule is unstable but the decay rate is vanishing, the survival probability $P(t)$ follows to a very good approximation a stretched-exponential law $P(t) = \exp(-a\sqrt{t})$. Forerunners of the stretched-exponential decay can be observed in the transient parts of decays with $\gamma \neq 0$, when B approaches B_1 .

survival probability (69) is determined by the form of the energy density close to the origin

$$P(t) \simeq \left| \int_0^\infty dE \frac{\sqrt{E}}{(E + E_1)(E + E_2)} e^{-iEt/\hbar} \right|^2 \simeq \exp\left(-\sqrt{\frac{8t}{\pi\hbar}}(\sqrt{E_1} + \sqrt{E_2})\right) \left[1 + O\left(\frac{tE_2}{\hbar}\right)\right], \quad (72)$$

where E_1 and E_2 , with $E_1 < E_2$, are the absolute values of the (real and negative) poles of the analytic continuation of the propagator. Close to resonance, where $E_1 \rightarrow 0$, the decay constant and the range of validity of the stretched-exponential approximation are determined by the largest pole, which is more stable with respect to variations of the magnetic field. Moreover, it is worth observing that, even when the molecular state becomes stable, the stretched exponential survives at the beginning of the time evolution, before the system relaxes towards the stable state. On the other hand, as already outlined, a stretched-exponential behavior precedes the exponential decay also for $B > B_1$. Therefore, although the observation of this peculiar regime is limited, in a strict sense, to a range of magnetic field of order $10 \mu\text{G}$, a finer tuning of the magnetic field is not required to observe it.

Finally, it is worth recalling that a stretched-exponential law also appears in classical statistical mechanics as an average effect over many exponential decays with different rates [39]. Here, however, the effect is quantum mechanical and is the result of an interference of amplitudes, as shown in (72).

A final comment is in order, concerning the relation between our results, obtained by considering the evolution of a single molecule in vacuum, with the many-body physics of gas clouds, in which the phenomenology of Feshbach resonances is usually observed. Actually, even under the hypothesis of an initially dilute molecular gas, the fermionic

decay products can saturate the density of states

$$\rho(E) = \frac{m^{3/2} \sqrt{2E}}{2\pi^2 \hbar^2}, \quad (73)$$

giving rise to statistical effects. A *strong* condition for the validity of the single-molecule approximation at a time t^* consists in requiring that the density of products, estimated from the survival probability, the initial density of the molecule n_{mol} , and the energy density, satisfies

$$2n_{\text{mol}}[1 - P(t)]\omega(E) \lesssim \rho\left(\frac{E}{2}\right) \quad \text{for } t \leq t^*, E > 0. \quad (74)$$

However, in the most interesting case of stretched-exponential decay, with the magnetic field very close to the resonance, such a strong condition can be too limiting, since the energy density tends to become very large close to the origin. Nonetheless, the *weaker* condition that (74) be valid for $E \gtrsim E_2$ and $t \leq t^* \ll \hbar/E_2$ ensures that the single-molecule approximation is justified in the times of interest for the observation of the stretched exponential, in which the emission of particles with $E \lesssim E_2/2$ is suppressed.

VIII. CONCLUSION AND OUTLOOK

We have analyzed the time evolution of an unstable Feshbach molecule decaying into a pair of fermionic atoms with opposite momenta. We have shown that, while the decay is exponential for magnetic fields far from resonance, when the magnetic field approaches the resonance value, the decay is dominated by a stretched-exponential law $P(t) \simeq \exp(-a\sqrt{t})$.

Stretched exponentials appear in the phenomenological description of a variety of physical phenomena, in classical statistical physics, glassy dynamics, and low-energy one-

dimensional Bose gases [39–41]. They are often used to describe relaxation in disordered or complex systems, when different local dynamics give rise to superpositions of simple exponential decays, whose average effect yields stretched-exponential behavior. However, the stretched-exponential law unearthed in this article has a purely quantum-mechanical origin, being the consequence of interfering quantum amplitudes. The appearance of a stretched-exponential relaxation in the context described in the present article is therefore of interest, in that it bridges the gap between complexity and typical quantum relaxation phenomena in a cold gas.

We leave for future work the study of the time evolution of cold atomic systems in the presence of collective effects, such as macroscopic quantum tunneling in mixtures of Bose-Einstein condensates [52], confined in arbitrary potentials [53,54]. It would be interesting to understand whether curious time evolutions like the one analyzed in this work are present in different quantum situations.

ACKNOWLEDGMENTS

P.F. and S.P. were partially supported by Istituto Nazionale di Fisica Nucleare (INFN) through the project “QUANTUM.” F.V.P. was supported by INFN through the project “PICS.” P.F. was partially supported by the Italian National Group of Mathematical Physics of Istituto Nazionale di Alta Matematica (GNFM-INdAM). Z.K. thanks the Abdus Salam ICTP for their financial support through a TRIL Fellowship. Z.K. would also like to thank INFN, Bari, for the hospitality. P.F., F.V.P. and S.P. acknowledge support by MIUR via PRIN 2017 (Progetto di Ricerca di Interesse Nazionale), project QUSHIP (2017SRNBRK). F.V.P. acknowledges support by MIUR through PON ARS 01_00141 CLOSE.

-
- [1] G. Gamow, Zur quantentheorie des atomkernes, *Z. Phys.* **51**, 204 (1928).
 - [2] V. Weisskopf and E. Wigner, Berechnung der natürlichen linienbreite auf grund der Diracschen lichttheorie, *Z. Phys.* **63**, 54 (1930).
 - [3] V. Weisskopf and E. Wigner, Über die natürliche linienbreite in der strahlung des harmonischen oszillators, *Z. Phys.* **65**, 18 (1930).
 - [4] H. Nakazato, M. Namiki, and S. Pascazio, Temporal behavior of quantum mechanical systems, *Int. J. Mod. Phys. B* **10**, 247 (1996).
 - [5] P. Facchi and S. Pascazio, in *Progress in Optics*, edited by E. Wolf (Elsevier, Amsterdam, 2001), Vol. 42, Chap. 3, p. 147.
 - [6] P. Facchi and S. Pascazio, Quantum Zeno dynamics: Mathematical and physical aspects, *J. Phys. A: Math. Theor.* **41**, 493001 (2008).
 - [7] P. Facchi and M. Ligabò, Quantum Zeno effect and dynamics, *J. Math. Phys.* **51**, 022103 (2010).
 - [8] L. A. Khal'fin, On the theory of the decay of a quasi-stationary state, *Sov. Phys. Dokl.* **2**, 340 (1957).
 - [9] L. A. Khal'fin, Contribution to the decay theory of a quasi-stationary state, *Sov. Phys. JETP* **6**, 1053 (1958).
 - [10] P. Exner, *Open Quantum Systems and Feynman Integrals* (Reidel, Dordrecht, 1985).
 - [11] J. Martorell, J. G. Muga, and D. W. L. Sprung, in *Time in Quantum Mechanics - Vol. 2*, edited by J. G. Muga, A. Ruschhaupt, and A. del Campo, Lecture Notes in Physics Vol. 789 (Springer, Berlin, 2009), p. 239.
 - [12] D. Burgarth and P. Facchi, Positive Hamiltonians can give purely exponential decay, *Phys. Rev. A* **96**, 010103(R) (2017).
 - [13] E. B. Norman, S. B. Gazes, S. G. Crane, and D. A. Bennett, Tests of the Exponential Decay Law at Short and Long Times, *Phys. Rev. Lett.* **60**, 2246 (1988).
 - [14] D. Novković, L. Nadder, A. Kandić, I. Vukanac, M. Durašević, and D. Jordanov, Testing the exponential decay law of gold ^{198}Au , *Nucl. Instrum. Methods Phys. Res. Sect. A* **566**, 477 (2006).
 - [15] S. R. Wilkinson, C. F. Bharucha, M. C. Fischer, K. W. Madison, P. R. Morrow, Q. Niu, B. Sundaramand, and M. G. Raizen, Experimental evidence for non-exponential decay in quantum tunneling, *Nature (London)* **387**, 575 (1997).
 - [16] E. W. Streed, J. Mun, M. Boyd, G. K. Campbell, P. Medley, W. Ketterle, and D. E. Pritchard, Continuous and Pulsed Quantum Zeno Effect, *Phys. Rev. Lett.* **97**, 260402 (2006).

- [17] J.-M. Raimond, C. Sayrin, S. Gleyzes, I. Dotsenko, M. Brune, S. Haroche, P. Facchi, and S. Pascazio, Phase Space Tweezers for Tailoring Cavity Fields by Quantum Zeno Dynamics, *Phys. Rev. Lett.* **105**, 213601 (2010).
- [18] F. Schäfer, I. Herrera, S. Cherukattil, C. Lovecchio, F. S. Cataliotti, F. Caruso, and A. Smerzi, Experimental realization of quantum Zeno dynamics, *Nat. Commun.* **5**, 3194 (2014).
- [19] A. Signoles, A. Facon, D. Grosso, I. Dotsenko, S. Haroche, J.-M. Raimond, M. Brune, and S. Gleyzes, Confined quantum Zeno dynamics of a watched atomic arrow, *Nat. Phys.* **10**, 715 (2014).
- [20] G. Barontini, L. Hohmann, F. Haas, J. Estève, and J. Reichel, Deterministic generation of multiparticle entanglement by quantum Zeno dynamics, *Science* **349**, 1317 (2015).
- [21] Y. Lin, J. P. Gaebler, F. Reiter, T. R. Tan, R. Bowler, Y. Wan, A. Keith, E. Knill, S. Glancy, K. Coakley, A. S. Sørensen, D. Leibfried, and D. J. Wineland, Preparation of Entangled States through Hilbert Space Engineering, *Phys. Rev. Lett.* **117**, 140502 (2016).
- [22] M. C. Fischer, B. Gutiérrez-Medina, and M. G. Raizen, Observation of the Quantum Zeno and Anti-Zeno Effects in an Unstable System, *Phys. Rev. Lett.* **87**, 040402 (2001).
- [23] A. Crespi, F. V. Pepe, P. Facchi, F. Sciarrino, P. Mataloni, H. Nakazato, S. Pascazio, and R. Osellame, Experimental Investigation of Quantum Decay at Short, Intermediate, and Long Times via Integrated Photonics, *Phys. Rev. Lett.* **122**, 130401 (2019).
- [24] A. Crespi, F. V. Pepe, P. Facchi, F. Sciarrino, P. Mataloni, H. Nakazato, S. Pascazio, and R. Osellame, Experimental investigation of quantum decay via integrated photonics, *MDPI Proc.* **12**, 9 (2019).
- [25] C. Chin, R. Grimm, P. Julienne, and E. Tiesinga, Feshbach resonances in ultracold gases, *Rev. Mod. Phys.* **82**, 1225 (2010).
- [26] T. Kostyrko and J. Ranninger, Spectral properties of the boson-fermion model in the superconducting state, *Phys. Rev. B* **54**, 13105 (1996).
- [27] A. Perali, P. Pieri, G. C. Strinati, and C. Castellani, Pseudogap and spectral function from superconducting fluctuations to the bosonic limit, *Phys. Rev. B* **66**, 024510 (2002).
- [28] P. Pieri, L. Pisani, and G. C. Strinati, BCS-BEC crossover at finite temperature in the broken-symmetry phase, *Phys. Rev. B* **70**, 094508 (2004).
- [29] C. A. R. Sá de Melo, M. Randeria, and J. R. Engelbrecht, Crossover from BCS to Bose Superconductivity: Transition Temperature and Time-Dependent Ginzburg-Landau Theory, *Phys. Rev. Lett.* **71**, 3202 (1993).
- [30] C. Samuelis, E. Tiesinga, T. Laue, M. Elbs, H. Knöckel, and E. Tiemann, Cold atomic collisions studied by molecular spectroscopy, *Phys. Rev. A* **63**, 012710 (2000).
- [31] A. D. Lange, K. Pilch, A. Prantner, F. Ferlaino, B. Engeser, H.-C. Nägerl, R. Grimm, and C. Chin, Determination of atomic scattering lengths from measurements of molecular binding energies near Feshbach resonances, *Phys. Rev. A* **79**, 013622 (2009).
- [32] S. J. J. M. F. Kokkelmans, H. M. J. Vissers, and B. J. Verhaar, Formation of a Bose condensate of stable molecules via a Feshbach resonance, *Phys. Rev. A* **63**, 031601(R) (2001).
- [33] T. Hornung, S. Gordienko, R. de Vivie-Riedle, and B. J. Verhaar, Optimal conversion of an atomic to a molecular Bose-Einstein condensate, *Phys. Rev. A* **66**, 043607 (2002).
- [34] T. Yamakoshi, S. Watanabe, C. Zhang, and C. H. Greene, Stochastic and equilibrium pictures of the ultracold Fano-Feshbach-resonance molecular conversion rate, *Phys. Rev. A* **87**, 053604 (2013).
- [35] R. A. Duine and H. T. C. Stoof, Atom-molecule coherence in Bose gases, *Phys. Rep.* **396**, 115 (2004).
- [36] G. E. Cragg and A. K. Kerman, Coherent Decay of Bose-Einstein Condensates, *Phys. Rev. Lett.* **98**, 080405 (2007).
- [37] K. E. Strecker, G. B. Partridge, and R. G. Hulet, Conversion of an Atomic Fermi Gas to a Long-Lived Molecular Bose Gas, *Phys. Rev. Lett.* **91**, 080406 (2003).
- [38] A. J. Moerdijk, B. J. Verhaar, and A. Axelsson, Resonances in ultracold collisions of ${}^6\text{Li}$, ${}^7\text{Li}$, and ${}^{23}\text{Na}$, *Phys. Rev. A* **51**, 4852 (1995).
- [39] D. C. Johnston, Stretched exponential relaxation arising from a continuous sum of exponential decays, *Phys. Rev. B* **74**, 184430 (2006).
- [40] M. Mézard, G. Parisi, and M. Á. Virasoro, *Spin Glass Theory and Beyond* (World Scientific, Singapore, 1987).
- [41] J.-S. Bernier, R. Citro, C. Kollath, and E. Orignac, Correlation Dynamics During a Slow Interaction Quench in a One-Dimensional Bose Gas, *Phys. Rev. Lett.* **112**, 065301 (2014).
- [42] M. Holland, S. J. J. M. F. Kokkelmans, M. L. Chiofalo, and R. Walser, Resonance Superfluidity in a Quantum Degenerate Fermi Gas, *Phys. Rev. Lett.* **87**, 120406 (2001).
- [43] Y. Ohashi and A. Griffin, Superfluidity and collective modes in a uniform gas of Fermi atoms with a Feshbach resonance, *Phys. Rev. A* **67**, 063612 (2003).
- [44] G. M. Bruun and C. J. Pethick, Effective Theory of Feshbach Resonances and Many-Body Properties of Fermi Gases, *Phys. Rev. Lett.* **92**, 140404 (2004).
- [45] A. L. Fetter and J. D. Walecka, *Quantum Theory of Many-Particle Systems* (Dover, New York, 2003).
- [46] I. Bloch, J. Dalibard, and W. Zwerger, Many-body physics with ultracold gases, *Rev. Mod. Phys.* **80**, 885 (2008).
- [47] C. Cohen-Tannoudji, J. Dupont-Roc, and G. Grynberg, *Atom-Photon Interactions: Basic Processes and Applications* (Wiley-VCH, Weinheim, 1998).
- [48] L. Pricoupenko and M. Jona-Lasinio, Ultracold bosons in the vicinity of a narrow resonance: Shallow dimer and recombination, *Phys. Rev. A* **84**, 062712 (2011).
- [49] E. Braaten and H.-W. Hammer, Universality in few-body systems with large scattering length, *Phys. Rep.* **428**, 259 (2006).
- [50] P. Facchi, H. Nakazato, and S. Pascazio, From the Quantum Zeno to the Inverse Quantum Zeno Effect, *Phys. Rev. Lett.* **86**, 2699 (2001).
- [51] A. Crespi, F. V. Pepe, P. Facchi, F. Sciarrino, P. Mataloni, H. Nakazato, S. Pascazio, and R. Osellame, *Quantum Information and Measurement (QIM) V: Quantum Technologies*, OSA Technical Digest (Optical Society of America, Washington, DC, 2019), paper T5A.4.
- [52] K. Kasamatsu, Y. Yasui, and M. Tsubota, Macroscopic quantum tunneling of two-component Bose-Einstein condensates, *Phys. Rev. A* **64**, 053605 (2001).
- [53] P. Facchi, G. Florio, S. Pascazio, and F. V. Pepe, Binary mixtures of condensates in generic confining potentials, *J. Phys. A: Math. Theor.* **44**, 505305 (2011).
- [54] F. V. Pepe, P. Facchi, G. Florio, and S. Pascazio, Domain wall suppression in trapped mixtures of Bose-Einstein condensates, *Phys. Rev. A* **86**, 023629 (2012).